Free Space Detection from Catadioptric Omnidirectional Images for Visual Navigation using Optical Flow

Wataru Yoshizaki, Yoshihiko Mochizuki, Naoya Ohnishi, Atsushi Imiya

Free Space Detection from Catadioptric Omnidirectional Images for Visual Navigation using Optical Flow

Wataru Yoshizaki[1] *, Yoshihiko Mochizuki[2], Naoya Ohnishi[3] **
, and Atsushi Imiya[4]

[1] Dept. of Information and Image Science, Faculty of Engineering, Chiba University, Japan
[2] School of Advanced Integration Science, Chiba University, Japan
[3] School of Science and Technology, Chiba University, Japan
[4] Institute of Media and Information Technology, Chiba University, Japan
Yayoicho 1-33, Inage-ku, Chiba, 263-8522, Japan

Abstract. In this paper, we develop a free space detection algorithm for the visual navigation of the autonomous robot mounting a catadioptiric omnidirectional imaging system. The algorithm detects the dominant plane as the free space from a sequence of omnidirectional images captured by a camera mounted on the autonomous robot. The dominant plane, which can be detected from the optical-flow field, is the largest planar area in the image. For the detection of the dominant plane from the optical-flow field, we adopt the motion separation property, that is, the optical-flow vector is decomposed into infinitesimal rotation, translation, and divergent motions on the images. The algorithm matches the measured translation optical-flow field with the template translation optical-flow field to separate the dominant-plane as the free space for the navigation and the obstacle area. The template optical-flow field is generated from a preobserved image sequence without any calibration of the internal parameters of both the robot and camera.

1 Introduction

In this paper, we develop the dominant-plane-based [15] free-space-detection algorithm for the autonomous robot mounting a catadioptric omnidirectional imaging system. A featureless and uncalibrated visual navigation for the pinhole camera system is developed by Santos-Victor and Sandini, [18] and by Ohnishi and Imiya [15]. The former is a model-based method and the latter is a non-model-based method. The latter method detects the free space for the robot navigation using the optical-flow field computed from images captures by the

* Present Address: Graduate School of Information Science NAIST, Takayama 8916-5, Ikoma, NARA, 630-0192, Japan
** Present Address: Power and Industry Systems Research and Development Centers, Power Systems Company, TOSHIBA, Fuchu, Tokyo, Japan

imaging system mounted on the autonomous robot [4, 5], although both methods compute free space from the optical-flow field. The former method generates the model optical-flow field in the pretuning process using images without any obstacles. In this paper, we extend the dominant-plane-detection navigation to the autonomous robot mounting a catadioptric omnidirectional vision system [2, 5, 8, 14], that is, we use optical-flow field [1, 3, 11, 13] on the omnidirectional images for the detection of the dominant plane as the free space for the robot navigation.

For the extension of the previous featureless robot navigation strategy [18, 15] to the omnidirectional vision system, we adopt the motion separation property, that is, the optical-flow vector is decomposed into infinitesimal rotation, translation, and divergent motions on the images. This geometrical property is well studied on the pinhole camera system. We first clarify the motion separation property of the optical-flow vectors for the omnidirectional images. Then, using this geometrical property of the optical-flow vectors, we develop a free space detection algorithm for the omnidirectional images. In our algorithm, the measured translation optical-flow field of the omnidirectional image is matched with the template translation optical-flow field [18], which is generated from a preobserved omnidirectional image sequence, to separate the dominant plane as the free space for the navigation and the obstacle area. Therefore, the output of the algorithm for the navigation is binary images which express the free space and the obstacle area.

The robot navigation in an environment without any landmarks, such as a new environment without any configuration maps for the robot, the detection of the free space, in which the robot can move without any colliding with the obstacles, is a fundamental task. Ohnishi and Imiya [15], Sobey [17], Santos-Victor [18] and Braillon et al. [4] developed an algorithm for the free space detection using optical-flow vectors [17, 18] and a sequence of optical-flow field [15], since the autonomous robot with a vision system automatically detects a sequence of images from the vision system mounted on the robot.

The omnidirectional vision system is widely used in the surveillance systems and robot navigation systems [8, 12, 20]. Using the wide view of the omnidirectional imaging system, in the surveillance and navigation, the moving objects and the landmarks in the wide area are detected for inspection and robot localisation, respectively. For the robot navigation, the omnidirectional or panoramic views allow the simple computation for localisation of the robot using the several landmarks in the omnidirections detected simultaneously by a single camera. This geometrical advantage is the most important property of the omnidirectional imaging system mounted on the autonomous robot for the navigation and localisation.

In a real environment, the payload of a mobile robot, for example, the power supply, capacity of input devices and computing power, is restricted. Therefore, mobile robots are required to have simple mechanisms and devices [10, 15] for the navigation and localisation. We use an uncalibrated monocular camera as a sensor for obtaining information on the environment. This vision sensor is a

low-cost device that is easily mounted on mobile robots. Therefore, we use visual information for the mobile robot navigation.

As same as the pinhole camera system, geometrical features such as lines and planes in the environment are fundamental cues for the panoramic and omnidirectional vision systems to detect the configuration of obstacles in the three-dimensional workspace. If we adopt these traditional strategies, the robot is required to detect the free space as the dual area of the space occupied by obstacle objects. Furthermore, if the map of the workspace is used for the navigation, the robot is required to prepare a geometrical transformation method for transforming the omnidirectional views to the map and reversely to generate omnidirectinal views from the map for the localisation of the robot in the workspace. These two methodologies request for the robot to prepare the special memories for the visual navigation. Therefore, the featureless method developed for the pinhole camera system is suitable for the small payload robot mounting an omnidirectional imaging system, since the algorithm is simple.

Ohnishi and Imiya [15], developed a featureless robot navigation method based on a planar area and an the optical-flow field computed from a pair of successive images. A planar area in the three-dimensional space is called a dominant plane, if it occupies the largest part of an image. We first accept the following four assumptions used by Ohnishi and Imiya [15].

1. The ground plane is the planar area.
2. The camera mounted on a mobile robot is downward-looking.
3. The robot observes the world using the camera mounted on itself for navigation.
4. The camera on the robot captures a sequence of images since the robot is moving.

For the autonomous robot mounting an omni directional camera system, we add the following two assumptions for the camera configuration.

5. The optical axis of the catadioptric omni-directional system mounted on the robot is perpendicular to the ground flow.
6. The planar area occupies more than three fourth of the image.

Although the property of item 5 is the results of the camera-mounting geometry, item 6 is the requirement for the motion separation property on the image. Therefore, if there are no obstacles around the robot and the robot does not touch the obstacles, the ground plane corresponds to the dominant plane in the image observed through the camera mounted on the mobile robot.

Using a vision system inspired by insects, navigation algorithms for the autonomous robot are proposed [6, 7, 9, 17, 19]. The insect-inspired vision for robot control uses simple information observed by the vision system mounted on the robot. The optical-flow field is a feature computed from an image sequence observed form the moving camera. Therefore, the optical-flow field is a fundamental simple cue for controlling autonomous vehicles [4, 9].

Sobey [17] introduced a control strategy for robot navigation using optical flow and the potential field, using the relationship between optical flow and range,

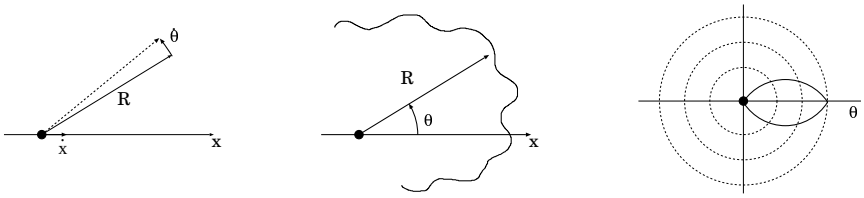

(a) (b) (c)

Fig. 1. Insect-inspired range navigation. (a)–(c) Insect inspired range potential. An insect understands the range data in the eye-centred coordinates using the optical flow field observed while it is flying around the environment. This range data observed by the moving camera (eye) yields the range-based potential field around the insect for navigation to the local destination. (a) Motion and optical flow. (b) Range data in the eye-centred coordinate. (c) The range-based potential for control to the local destination. In these figures, $\dot{\boldsymbol{x}}$, $\dot{\theta}$, and R are the velocity of the insect, the angular velocity of objects, and the distance to the object, respectively. Then, the relationship $\dot{\theta} = \dot{\boldsymbol{x}} \frac{\sin\theta}{R}$ is satisfied.

which is possibly used by insects for the detection of obstacles in the space for motion control, as shown in Fig. 1. This range in the space detected by the optical flow observed by the camera is used for the generation of the potential, which is used for the computation of the control force to avoid colliding with obstacles. The view from the eyes of flying birds and the compound eyes of insects is a spherical image, which is a standard normalised image for images captured by the omnidirectional vision system. The catadioptric omnidirectional system is widely used in robot vision. In this, paper, we develop an algorithm for the catadioptric imaging system to the detection of free space for the robot navigation without reconstructing three-dimensional geometry of obstacles in the workspace. Therefore, the algorithm is simple and suitable for a low-payload autonomous mobile robot.

2 Motion Separation and Dominant Plane

2.1 Imaging geometry

In this paper, we assume that the catadioptric camera is that with the hyperbolic mirror which is expressed as

$$-\frac{x^2+y^2}{a^2}+\frac{z^2}{b^2}=1. \tag{1}$$

For this hyperbola, setting $f_z = \sqrt{a^2+b^2}$ a pair of points $P_{F1} = (0,0,f_z)^\top$ and $P_{F2} = (0,0,-f_z)^\top$ are the focal points of this hyperbola. We use the positive

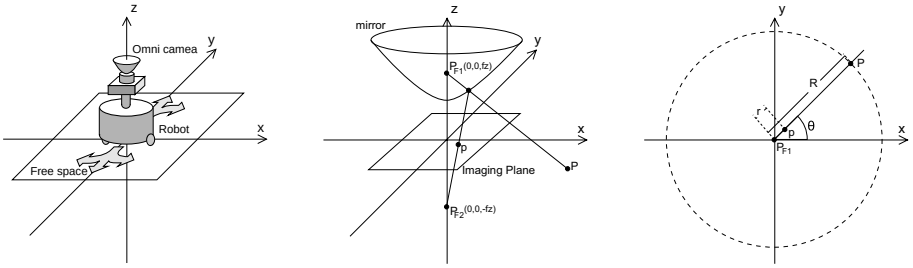

(a) Robot motion (b) Imaging geometry (c) Coordinate system

Fig. 2. Geometry of the catadioptric camera system. The robot mounting a catadioptric omnidirectional system moves on the ground floor. The optical axis of the camera system is perpendicular to the ground floor. The robot moves as the combination of the rotation around the gravity axis of the robot and the translation. The focal point $(0, 0, f_s)^\top$ of the pinhole camera is located on the focal point of the hyperbola P_F.

hyperbola $z > 0$ as the mirror of a catadioptric imaging system, and we locate the focal point of the pin-hole camera on the focal point of the hyperbola $(0, 0, -P_F)$.

For the analysis of the optical-flow vector caused by the rotation and translation of the robot as shown in Fig. 2(a), we adopt the cylindrical coordinate system to express the location of the point $\boldsymbol{P}$ in the space as $\boldsymbol{P} = (R\cos\theta, R\sin\theta, Z)^\top$. In the catadioptric imaging system, the point $\boldsymbol{P}$ in the space is transformed to the point

$$\boldsymbol{p} = (r\cos\theta, r\sin\theta)^\top = r\boldsymbol{n} \tag{2}$$

on the imaging plane, for

$$r = \frac{f_z}{z + f_z} q,\ q = a^2 \frac{-f_z\gamma + \sqrt{b^2(\gamma^2 + 1)}}{a^2\gamma^2 - b^2},\ z = q\gamma + f_z,\ \gamma = \frac{f_z - Z}{R}. \tag{3}$$

This transformation is geometrically shown in Figs. 2(b) and 2(c). Equation (3) implies that the points $\boldsymbol{P} = (R\cos\theta, R\sin\theta, Z)^\top$ and $\boldsymbol{P'} = (R'\cos\theta, R'\sin\theta, Z')^\top$ are imaged to the same point $\boldsymbol{p} = (r\cos\theta, r\sin\theta)^\top$ if two points satisfy the condition $\frac{f_z - Z}{R} = \frac{f_z - Z'}{R'}$.

2.2 Optical flow separation

The optical-flow vector is the appearance motion on an image computed from a sequence of images. Optical-flow vectors are the projections of the infinitesimal motion vectors in the space onto the imaging plane.

The projection of the infinitesimal motion in the space onto the imaging plane is the optical-flow vector. Assuming that the point $\boldsymbol{P}$ moves to $\boldsymbol{P'} = \boldsymbol{P} + \boldsymbol{\Delta}$ during Δt, we compute the difference of a pair of points $\boldsymbol{p}$ and $\boldsymbol{p'}$ on the imaging

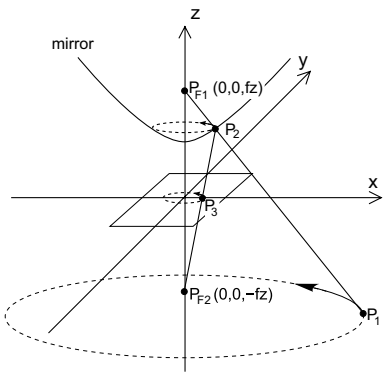

(a) The point motion by the rotation of the robot

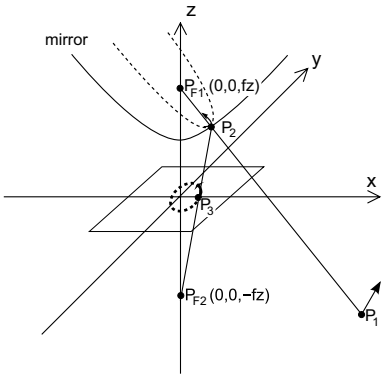

(b) The point motion by the translation of the robot

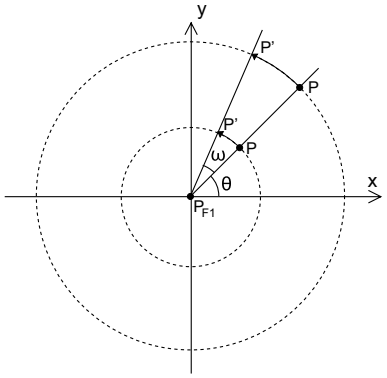

(c) Optical-flow by the rotation of the robot

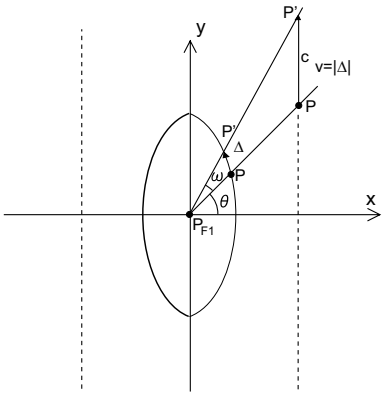

(d) Optical-flow by the translation of the robot

Fig. 3. The projection of the infinitesimal motion in the space onto the imaging plane is the optical-flow vector. (a) The rotation of the robot causes the rotation optical-flow. The rotation optical flow is the tangent vectors to the cocentred circles around the optical axis of the catadioptric camera. For the rotation, the angle $\angle[P'P_{F1}P']$ is constant. (b) The translation of the robot causes the translation optical-flow. The translation optical flow is the tangent vector to the bundle of elliptic arcs which is the projection of the bundle of parallel lines in the space. For the translation motion, the length of the line segment $\overline{P'P} = c$ is constant, where $|\boldsymbol{\Delta}| \cos\theta = \frac{\omega D}{\cos\theta}$.

plane which are the projections of points $\boldsymbol{P}$ and $\boldsymbol{P'} = (\boldsymbol{P} + \boldsymbol{\Delta})$, respectively. The optical-flow vector $\boldsymbol{u}$ is computed as

$$\boldsymbol{u} = \frac{\Delta \boldsymbol{p}}{\Delta t} = \boldsymbol{p'} - \boldsymbol{p} = \{\text{the image of } \boldsymbol{\Delta}\} = \{\text{the image of } (\boldsymbol{P'} - \boldsymbol{P})\}. \quad (4)$$

The optical-flow vector is decomposed to the rotation, translation, and divergent vectors as

$$\boldsymbol{u} = \boldsymbol{u}_r + \boldsymbol{u}_t + \boldsymbol{u}_d. \quad (5)$$

The rotation vector $\boldsymbol{u}_r$ is caused by the rotation of the imaging system around the optical axis of the imaging system. The translation vector $\boldsymbol{u}_t$ is caused by the translation of the optical centre parallel to a plane. The divergent vector $\boldsymbol{u}_d$ is caused by the motion of the optical centre toward the infinite point in the space.

In this paper, we assume that a catadioptric omnidirectional camera system is mounted on the robot as shown in Fig. 2. The camera observes the vector bundle caused by the translation and rotation of the robot. In this camera configuration, for any camera motion caused by the robot drive, the camera centre does not move in the direction of the optical axis of the camera. Therefore, the camera does not observe the divergent vector bundle as part of the appearance motion.

2.3 Rotation optical flow

From eq. (3), we have the relation that $\frac{\partial}{\partial \theta} r = 0$. Therefore, if the point $\boldsymbol{P} = (R\cos\theta, R\sin\theta, Z)^\top$ moves to the point $\boldsymbol{P'} = (R\cos(\theta+\omega), R\sin(\theta+\omega), Z)^\top$ for a small angle ω, the optical-flow vector on the imaging plane is computed as

$$\boldsymbol{u}(r,\theta) = \boldsymbol{p'} - \boldsymbol{p} = \omega r \boldsymbol{n}^\perp \quad (6)$$

for $\boldsymbol{n}^\perp = (-\sin\theta, \cos\theta)^\top$. Therefore, the optical flow of the rotation of the robot is a collection of co-centred circles on the imaging plane as shown in Figs. 3(a) and 3(c). Furthermore, the speed is independent to the angle θ, that is, $\frac{\partial}{\partial \theta}|\boldsymbol{u}_r| = 0$. Moreover, we have the relation for the rotation angular velocity as

$$\omega = \frac{1}{r}|\boldsymbol{u}_r(r,\theta)|. \quad (7)$$

From eq. (6), we have the relation

$$\boldsymbol{u}(r,\theta+\pi) = -\boldsymbol{u}(r,\theta). \quad (8)$$

2.4 Translation opticalflow

The optical flow caused by the translation of the camera centre is the image of a line in the space. Assuming that the point $\boldsymbol{P} = (R\cos\theta, R\sin\theta, Z)^\top$ moves to $\boldsymbol{P'} = (R'\cos(\theta+\omega), R'\sin(\theta+\omega), Z)^\top$ with the constant speed $v = |\boldsymbol{\Delta}| = \omega\frac{D}{\cos^2\theta}$

in the direction $(0,1,0)^\top$, we set the projections of the pair of points $\boldsymbol{P}$ and $\boldsymbol{P}'$ as

$$\boldsymbol{p} = (r\cos\theta, r\sin\theta)^\top,\ \boldsymbol{p}' = (r'\cos(\theta+\omega), r'\sin(\theta+\omega))^\top. \tag{9}$$

The pair of points $\boldsymbol{P}$ and $\boldsymbol{P}'$ lie on the line $(D, D|\tan\theta|, Z)^\top$, $-\pi \le \theta \le \pi$.

From the camera geometry in Figs. 3(b) and 3(d), we have the relations

$$r = \frac{f_z}{f_z - Z}\ \frac{l - \frac{f_z(f_z-Z)}{b}}{l + \frac{f_z(f_z-Z)}{b}(3 - 2\frac{b^2}{a^2})}|\tan\theta|, \tag{10}$$

$$l = \sqrt{D^2\tan^2\theta + (f_z - Z)^2}, \tag{11}$$

$$r' = \frac{f_z}{f_z - Z}\ \frac{l' - \frac{f_z(f_z-Z)}{b}}{l' + \frac{f_z(f_z-Z)}{b}(3 - 2\frac{b^2}{a^2})}|\tan(\theta+\omega)|, \tag{12}$$

$$l' = \sqrt{D^2\tan^2(\theta+\omega) + (f_z - Z)^2}. \tag{13}$$

Using the relation

$$\begin{aligned}\frac{\Delta\boldsymbol{p}}{\Delta t} &= \boldsymbol{p}' - \boldsymbol{p} \\ &= \frac{f_z}{f_z - Z}\begin{pmatrix} \frac{(l' - \frac{f_z(f_z-z_1)}{b})}{l' + \frac{f_z(f_z-Z)}{b}(3-2\frac{b^2}{a^2})}\sin(\theta+\omega) - \frac{(l - \frac{f_z(f_z-Z)}{b})}{l + \frac{f_z(f_z-z_1)}{b}(3-2\frac{b^2}{a^2})}\sin\theta \\ \frac{(l' - \frac{f_z(f_z-Z)}{b})|\tan(\theta+\omega)|}{l' + \frac{f_z(f_z-Z)}{b}(3-2\frac{b^2}{a^2})}\sin(\theta+\omega) - \frac{(l - \frac{f_z(f_z-Z)}{b})\tan\theta}{l + \frac{f_z(f_z-Z)}{b}(3-2\frac{b^2}{a^2})}\sin\theta \end{pmatrix}\end{aligned} \tag{14}$$

for $R \cong R'$ and $\omega \ll 1$, we have the optical-flow vector on the imaging plane as

$$\boldsymbol{u}_t(r,\theta) = \omega d\cos\theta \begin{pmatrix} 1 \\ |\tan\theta| \end{pmatrix}, \tag{15}$$

where

$$d = \frac{f_z}{f_z - Z}\cdot\frac{l(\theta) - \frac{f_z(f_z-Z)}{b}}{l(\theta) + \frac{f_z(f_z-Z)}{b}(3 - 2\frac{b^2}{a^2})},\ l(\theta) = \sqrt{D^2\tan^2\theta + (f_z - Z)^2}. \tag{16}$$

From eq. (15), we have the relation

$$\boldsymbol{u}_t(r,\theta+\pi) = \boldsymbol{u}_t(r,\theta), \tag{17}$$

since $l(\theta+\pi) = l(\theta)$. The speed depends on the θ, that is, we have the relation $\frac{\partial}{\partial\theta}|\boldsymbol{u}_t| \neq 0$.

2.5 Motion separation

In Fig. 3, (a) shows that the rotation optical-flow vector which is the tangent vectors to the cocentred circles around the optical axis of the catadioptric camera. (b) shows that the translation optical-flow vector is the tangent vectors to

the bundle of elliptic arcs which is the projection of the bundle of parallel lines in the space.

From the analysis of the rotation and translation optical-flow vectors, we have the relations

$$\boldsymbol{u}_t(r,\theta) = \frac{1}{2}\boldsymbol{u}(r,\theta) + \boldsymbol{u}(r,\theta+\pi),\ \boldsymbol{u}_r(r,\theta) = \frac{1}{2}\boldsymbol{u}(r,\theta) - \boldsymbol{u}(r,\theta+\pi), \tag{18}$$

if there is no obstacles in the view. Furthermore, we have the relation for the rotation angular velocity as

$$\omega = \frac{1}{2r}|\boldsymbol{u}(r,\theta) - \boldsymbol{u}(r,\theta+\pi)|. \tag{19}$$

2.6 Dominant plane detection for omnidirectional images

For

$$\boldsymbol{P} = (D\tan\theta\cos\theta, D\tan\theta\sin\theta, Z)^\top,\ \boldsymbol{P}' = \boldsymbol{P} + \boldsymbol{\Delta}, \tag{20}$$

where $\boldsymbol{\Delta} = \Delta\boldsymbol{e}_2$ and $\boldsymbol{e}_2 = (0,1,0)^\top$ for a small positive number Δ and

$$\boldsymbol{Q} = \left(\frac{Z-s}{D}\tan\theta\cos\theta, \frac{Z-c}{Z}D\tan\theta\sin\theta, (Z-s)\right)^\top,\ \boldsymbol{Q}' = \boldsymbol{Q} + \boldsymbol{\Delta} \tag{21}$$

where $s > 0$, setting $\boldsymbol{p}$ and $\boldsymbol{q}$ to be the images of $\boldsymbol{P}$ and $\boldsymbol{Q}$, respectively, we have the relation,

$$\left|\frac{\Delta\boldsymbol{p}}{\Delta t}\right| < \left|\frac{\Delta\boldsymbol{q}}{\Delta t}\right|. \tag{22}$$

Therefore, the depth affects to the length of optical-flow vectors. This relation implies that we can discriminate optical-flow vectors on obstacle-region and the ground floor using the difference of the optical flow, if we have the optical-flow vectors on the ground floor.

If obstacles exist, we estimate the rotation velocity as

$$\bar{\omega} = \mathrm{Median}_{r,\theta}\left(\frac{1}{2r}|\boldsymbol{u}(r,\theta) - \boldsymbol{u}(r,\theta+\pi)|\right) \tag{23}$$

Then, we can separate the translation optical-flow vector of each point as

$$\overline{\boldsymbol{u}_t(r,\theta)} = \boldsymbol{u} - r\bar{\omega}\boldsymbol{n}^\perp. \tag{24}$$

Setting $\boldsymbol{u}_f(r,\theta)$ to be the optical-flow vectors computed from a pair of successive views without any obstacles, we have the relation

$$|\boldsymbol{u}_f(r,\theta) - \overline{\boldsymbol{u}_t(r,\theta)}| \le \varepsilon, \tag{25}$$

for a small positive constant at all points on the ground floor. This relation implies that, setting $\boldsymbol{u}_f(r,\theta)$ to be the template computed from views without any obstacles, we can detect the dominant plane as

$$D = \{(r\cos\theta, r\sin\theta)^\top \mid |\boldsymbol{u}_f(r,\theta) - \overline{\boldsymbol{u}_t(r,\theta)}| \le \varepsilon\}. \tag{26}$$

3 Numerical Results

For the validity evaluation of the method, we have evaluated the detection ratio of the dominant plane. For the qualitative analysis of the results, we used a synthetic environment generated in the computer and a synthetic image sequence observed from the camera mounted on the robot in the synthetic environment. Using 10 synthetic images for each speed, we have evaluated the following measures $E_1 = \frac{e_1}{N} \times 100[\%]$ and $E_2 = \frac{e_2}{N} \times 100[\%]$, where e_1, e_2, and N are the area in the free space detected as a part of obstacle area, the area in the obstacle area detected as a part of free space, and the area measure of the view, respectively.

For the computation of the optical-flow vectors on the imaging plane, we adopt the Lucas-Kanade mathod with Pyramid, LKP in abbreviation, for the optical flow computation [3] in the square grid on the imaging plane. The optical-flow vector decomposition compensates the accurate computation of the optical-flow for the dioptric omnidirectional images.

Table 1. Errors against speed of the robot τ. For $E_1 = \frac{e_1}{N} \times 100[\%]$ and $E_2 = \frac{e_2}{N} \times 100[\%]$, where e_1, e_2, and N are the area in the free space detected as a part of obstacle area, the area in the obstacle area detected as a part of free space, and the area measure of the view, respectively.

Dist.(mm)	Thd.$\epsilon = 0.3$px		Thd.$\epsilon = 0.5$px		Thd.$\epsilon = 0.7$px	
	E_1	E_2	E_1	E_2	E_1	E_2
5	51.6%	0.1%	25.6%	0.3%	13.0%	0.5%
10	25.9%	0.1%	8.9%	0.4%	4.3%	0.7%
15	13.8%	0.1%	4.3%	0.4%	2.4%	0.6%
20	8.1%	0.2%	2.8%	0.5%	1.9%	0.7%
25	6.2%	0.2%	2.6%	0.4%	1.9%	0.7%
30	5.5%	0.1%	2.5%	0.5%	1.8%	0.7%
35	4.8%	0.1%	2.3%	0.4%	1.8%	0.7%
40	5.1%	0.1%	2.5%	0.5%	1.9%	0.7%
45	4.8%	0.2%	2.4%	0.4%	1.9%	0.6%
50	5.2%	0.1%	2.7%	0.4%	2.1%	0.6%
55	4.8%	0.2%	3.0%	0.4%	2.5%	0.7%
60	4.7%	0.1%	3.0%	0.4%	2.6%	0.6%

These evaluations show that the estimated ratio is small for the speeds $20\text{mm/s} \leq v \leq 50\text{mm/s}$. This result is based on the property of the method as follows

- If the speed is too slow, the optical-flow vectors is inaccurately computed for the detection of the dominant plane and obstacles on the ominidirectional images using LKP.
- If the speed is too fast, LKP is unstable for the computation of the optical-flow vectors of the catadioptric omnidirectional images.

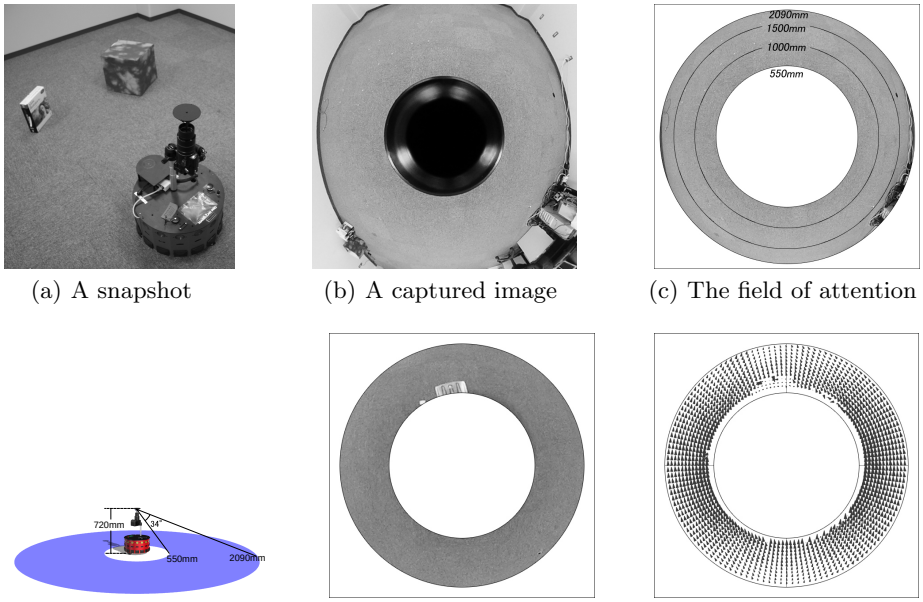

(a) A snapshot (b) A captured image (c) The field of attention

(d) View of the field of attention (e) An image (f) The template optical flow

Fig. 4. Geometric configuration of robot and template. (a) shows a snapshot of the work space. (b) is a captured image. (c) and (d) show the view fields of the robot. (e) and (f) show an observed image for the template optical-flow field computation and the template optical-flow field, respectively.

For the generation of the template, we used the area on the ground floor 550mm $\leq R \leq$ 2090mm centred at the rotation axis of the catadioptric camera. The geometrical configuration is shown in Fig. 4. In this figure, (a) shows a snapshot of the workspace (b) shows a captured image (c) and (d) show the view fields from the camera mounted on of the robot. (e) and (f) show an observed images for the template optical-flow vector computation and the template optical-flow, respectively. For the computation of the template optical-flow field, we set the translation distance $c = 10$mm/frame based on the performance evaluation by synthetic data.

Figure 5 shows a results. (a) is an image, (b) shows the optical-flow vectors, (c) the rotation optical-flow vectors, (d) shoes the translation optical-flow vectors, (e) shows the difference between the template optical-flow and translation optical-flow vectors, and (f) is the dominant plane (white area) and obstacles (grey area) detected by the image (e). In the experiment, we set $\varepsilon = 0.3$pixels These results show that our method detects the dominant plane from the catadioptric image sequence observed by the camera mounted on the autonomous

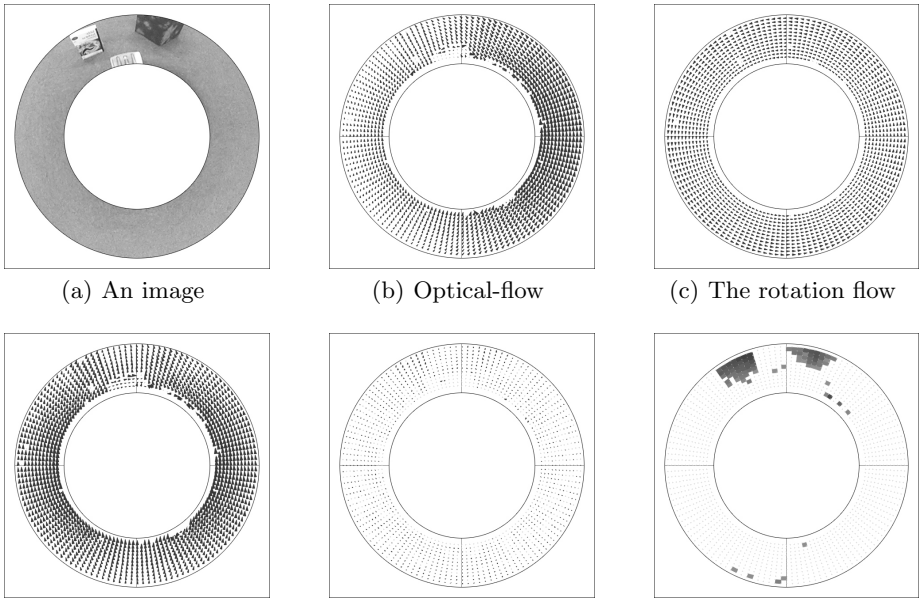

(a) An image (b) Optical-flow (c) The rotation flow

(d) The translation flow (e) Difference of the translation and the template(length × 3) (f) Dominant plane (white) and obstacles(gray)

Fig. 5. Result. (a)an image, (b)the optical-flow vectors, (c)the rotation optical-flow vectors, (d)the translation optical-flow vectors, (e)difference between the template optical-flow and translation optical-flow vectors, and (f)the dominant plane (white area) and obstacles (grey area) detected by the image (e).

robot. This result shows that our method detects the dominant plane as a free space from a catadioptric omni-directional images using optical flow.

Figure 6 shows a comparison evaluation of the method caused by the locations of obstacles in the workspace. In these results, images in the region $x \leq 0$ and $y \geq 0$ are shown, since the robot is moving in the direction $(-1, 0)^\top$ and the obstacles are located in the left of the robot. These three results show that the obstacles on the both side of the robot and close to the robot are accurately detected.

4 Conclusions

In this paper, we developed a featureless and uncalibration visual navigation algorithm for the robot mounting a catadioptric omnidirectional imaging system. Using optical flow, our algorithm detects the dominant plane as the free space from a sequence of omnidirectional images captured by an omnidirectional camera mounted on the autonomous robot. For the extension of the previous

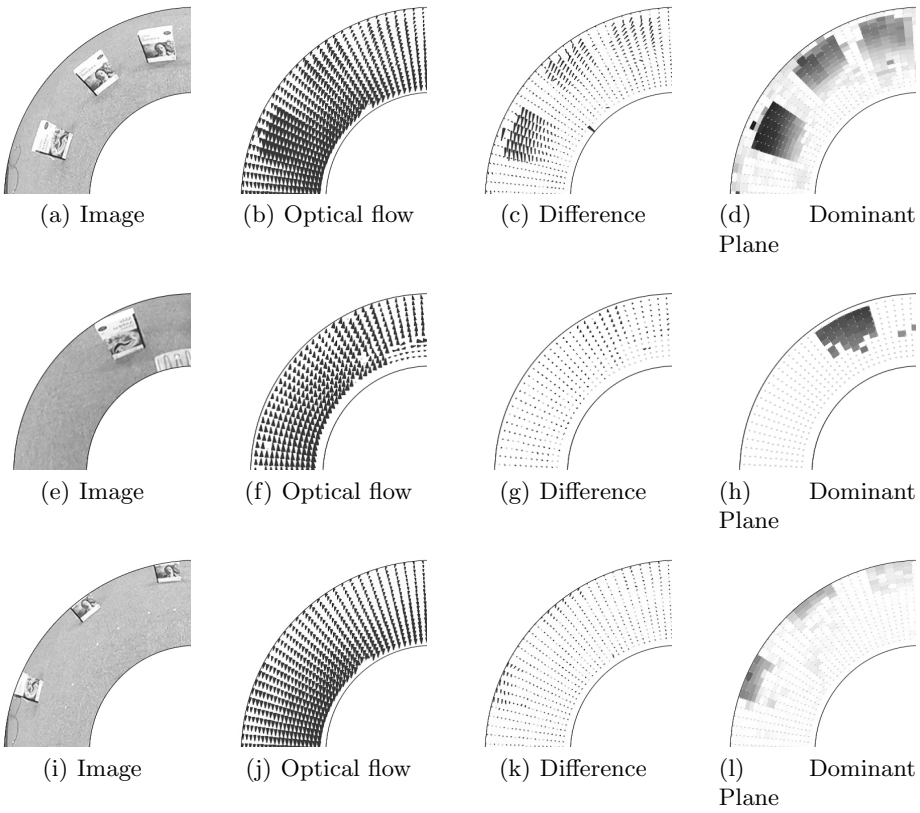

Fig. 6. Comparative examples. From left to right, the image, optical flow, difference with templates, and the dominant-plane, respectively. From top to bottom obstacles locate at 750mm (Three Boxes), 1200mmi (Two Boxes), and 1500mm (Three Boxes) from the centre of the coordinate system.

featureless and uncalibarated robot navigation strategies [18, 15] to the omnidirectional vision system, we adopt the motion separation property, that is, the optical-flow vector is decomposed into infinitesimal rotation, translation, and divergent motions on the images.

Using this geometrical property of the motion vector on the image, we developed an algorithm for the separation of the translation motion and rotation motion from a series of omnidirectional images. The magnitude of the motion vectors for translation motion depends on the range of the obstacles. Therefore, it is possible to separate the appearance motion vectors on an image computed from optical flow to motion on the ground floor and the motion on the obstacles. This property allowed the separation of the free space on an image. Since our algorithm requires template images from translating camera [18], we can con-

struct template for recognition without any calibration of internal parameters of both the robot and camera. in the pretuning process.

References

1. Barron, J.L., Fleet, D.J., Beauchemin, S.S., Performance of optical flow techniques, International Journal of Computer Vision, **12**, 43-77, 1994.
2. Barreto, J., Daniilidis, K., Unifying image plane liftings for central catadioptric and dioptric cameras, Proceedings of Omnivis04, 151-162, 2004.
3. Bouguet, J.-Y., Pyramidal implementation of the Lucas Kanade feature tracker description of the algorithm, Intel Corporation, Microprocessor Research Labs, OpenCV Documents, 1999.
4. Braillon, C., Pradalier, Ć., Crowley, J.L., Laugier, C., Real-time moving obstacle detection using optical flow models, Proceedings of Intelligent Vehicles Symposium, 466-471, 2006.
5. Bur, A., Tapus, A., Ouerhani, N., Siegwar, R., Hiigli, H., Robot navigation by panoramic vision and attention guided features, Proceedings of ICPR06, 695-698, 2006.
6. Franz, M. O., Mallot, H. A., Biomimetic robot navigation, Robotics and Autonomous Systems, **30**, 133-153, 2000.
7. Franz, M., Chahl, J., Krapp, H., Insect-inspired estimation of egomotion, Neural Computation, **16**, 2245-2260, 2004.
8. Gaspar, J., Winters, N., Santos-Victor, J., Vision-based navigation and environmental representations with an omnidirectional camera. IEEE Trans. Robotics and Automation, **16**, 890-898, 2000.
9. Green, W. E., Oh, P. Y., Barrows, G., Flying insect inspired vision for autonomous aerial robot maneuvers in near-earth environments, Proceedings of ICRA04, (2004)
10. Guilherme, N.D., Avinash, C.K., Vision for mobile robot navigation: A survey. IEEE Trans. on PAMI, **24**, 237-267, 2002.
11. Horn, B.K.P., Schunck, B.G., Determining optical flow. Artificial Intelligence, **17**, 185-203, 1981.
12. Lopez-Franco, C., Bayro-Corrochano, E., Omnidirectional vision and invariant theory for robot navigation using conformal geometric algebra, Proceedings of ICPR06, 570-573, 2006.
13. Lucas, B., Kanade, T.: An iterative image registration technique with an application to stereo vision. Proceedings of IJCAI, 674-679, 1981.
14. Nayar, S., Catadioptric omnidirectional cameras. Proceedings of CVPR97, 482-488, 1997.
15. Ohnishi, N., Imiya, A., Featureless robot navigation using optical flow. Connection Science, **17**, 23-46, 2000.
16. Ohnishi, N. Imiya, A., Dominant plane detection from optical flow for robot navigation. Pattern Recognition Letters, **27**, 1009-1021, 2006.
17. Sobey, P. J., Active navigation with a monocular robot, Biological Cybernetics, **71**, 433-440, 1994.
18. Santos-Victor, J. and Sandini, G., Uncalibrated obstacle detection using normal flow. Machine Vision and Applications, **9**, 130-137, 1996.
19. Vardy, A., Moller, R., Biologically plausible visual homing methods based on optical flow techniques. Connection Science, **17**, 47-89, 2005.
20. Winters, N., Gaspar, J., Lacey, J., Santos-Victor, J., Omni-directional vision for robot navigation. Proceedings of Omnivis00, 2000.